Biomaterials 104 (2016) 32–42

Contents lists available at ScienceDirect

Biomaterials

journal homepage: www.elsevier.com/locate/biomaterials

Optimizing growth and post treatment of diamond for high capacitance neural interfaces

Wei Tong [a], Kate Fox [b], Akram Zamani [c], Ann M. Turnley [c], Kumaravelu Ganesan [a], Arman Ahnood [a], Rosemary Cicione [a], Hamish Meffin [d], Steven Prawer [a], Alastair Stacey [a, 1], David J. Garrett [a, *, 1]

[a] School of Physics, University of Melbourne, Victoria 3010, Australia
[b] Centre for Additive Manufacturing, School of Engineering, RMIT University, Victoria 3001, Australia
[c] Department of Anatomy and Neuroscience, University of Melbourne, Victoria 3010, Australia
[d] National Vision Research Institute, Department of Optometry and Vision Science University of Melbourne, Victoria 3010, Australia

ARTICLE INFO

Article history:
Received 26 April 2016
Received in revised form
23 June 2016
Accepted 4 July 2016
Available online 6 July 2016

Keywords:
Nitrogen included ultrananocrystalline diamond
Oxygen plasma
Electrochemical capacitance
Neuron growth
Retinal implant

ABSTRACT

Electrochemical and biological properties are two crucial criteria in the selection of the materials to be used as electrodes for neural interfaces. For neural stimulation, materials are required to exhibit high capacitance and to form intimate contact with neurons for eliciting effective neural responses at acceptably low voltages. Here we report on a new high capacitance material fabricated using nitrogen included ultrananocrystalline diamond (N-UNCD). After exposure to oxygen plasma for 3 h, the activated N-UNCD exhibited extremely high electrochemical capacitance greater than 1 mF/cm^2, which originates from the special hybrid sp^2/sp^3 structure of N-UNCD. The *in vitro* biocompatibility of the activated N-UNCD was then assessed using rat cortical neurons and surface roughness was found to be critical for healthy neuron growth, with best results observed on surfaces with a roughness of approximately 20 nm. Therefore, by using oxygen plasma activated N-UNCD with appropriate surface roughness, and considering the chemical and mechanical stability of diamond, the fabricated neural interfaces are expected to exhibit high efficacy, long-term stability and a healthy neuron/electrode interface.

1. Introduction

Neural interfaces, also called brain-computer interfaces, which are formed at the interface of neural prosthesis and the neural tissues, hold the potential to treat or assist people with disabilities of neural function. Neural interfaces have the potential to restore or enhance the function of neural tissues which might be damaged or lost due to disease or injuries. Common targets for such devices are hearing loss [1], vision impairment [2,3] and paralysis [4,5]. Beyond medical applications, the emergence of neural interfaces offers the promise of technologies that formerly resided only in the realm of scientific fiction. For instance, the emergence of technologies that permit control of machines with our mind potentially frees us from the physical limitations of our bodies and could greatly increase our capabilities. Neural interfaces also offer a unique means to gather insight into our basic understanding of neurosciences, in particular insights concerning brain function and the mechanisms behind neural diseases.

The generation of action potentials by electrical stimulation or transduction of action potentials by electrical recording forms the basis of neural prosthetic interfaces [6]. The properties of electrodes at the interfaces for neural stimulation and recording are critical to the success of the devices. The selection of electrode material directly determines the efficacy, reliability and lifetime of the neural interfaces. Apart from the requirements of chemical and biochemical stability, it is necessary for the interfacing materials to be able to be processed into devices, exhibit robust mechanical stability and maintain electrochemical functionality within the harsh biological environment over the long term [7]. The biocompatibility of the interface material is another critical prerequisite in that any increase in distance formed between the electrodes and the target neural cells due to acute or chronic inflammation resulting in neuron loss may have adverse health outcomes and decreased neural functionality. These processes will ultimately

* Corresponding author.
E-mail address: d.garrett@unimelb.edu.au (D.J. Garrett).
[1] Denotes equal contribution from the authors.

http://dx.doi.org/10.1016/j.biomaterials.2016.07.006
0142-9612/

significantly degrade the performance of the electrodes [8,9]. For stimulation applications, any increase in the electrode to neuron distance will increase the current required for excitation [10] and when used for recording, the distance between the active neurons and the electrode is inversely related to the amplitude of the signals obtained [6]. In addition, meeting the requirements for the electrochemical properties of the electrodes is also pivotal. The capacitance and impedance at the electrode-tissue interface directly impacts the safety and efficacy of stimulation [11,12] and the quality of recording [13,14]; electrochemical reactions at the interface can lead to electrode dissolution [15] and production of chemical species that may be damaging to tissues [6,12]. Therefore, it is difficult to find a material to fulfill all these requirements, viz. biocompatibility, high charge injection capacity, low impedance, chemical and electrochemical stability, simultaneously.

Conventionally, neural electrodes have been fabricated using materials such as platinum [16], gold [17] and conducting polymers [14]. These have been demonstrated to record or stimulate neural activity both *in vitro* and *in vivo* [13,14,16,17]. There are however concerns when using these materials. For example, metals such as platinum and gold exhibit low charge injection limits and high impedance, which can be unsuitable for effective electrical stimulation and high quality recording, particularly when very small electrodes are employed [13]. In the case of conducting polymers, their mechanical properties are not ideal, as they are quite brittle [18,19]. Recently developed polymers, named "shape-memory polymers (SMPs), can change mechanical properties *in vivo* to improve the modulus and geometry match with body tissue after rigid insertion, thus reducing the damage to neural cells as can happen when implanting electrodes of stiff materials such as platinum and other metals [20,21]. However, the lack of electrochemical stability is another limiting problem when using conducting polymers for long-term neural interfaces [22]. Therefore, it is desirable to explore other materials with a combination of better intrinsic properties for the development of neural interfaces.

In comparison with the conventional materials used for neural interfaces, diamond possesses a number of desirable properties for advanced biomedical applications [23,24]. Diamond exhibits outstanding biochemical stability, chemical inertness and mechanical stability. Therefore devices fabricated from diamond are expected to operate steadily for longer periods of time than many other materials. Studies have shown that diamond produced by chemical vapor deposition (CVD) is highly biocompatible, eliciting a minimal immune response comparable to that of titanium [25] or medical grade silicone [26]. Diamond can promote the adhesion, proliferation and differentiation of various types of cells, including fibroblasts [27,28], osteoblasts [29] and many other cell lines [30,31]. By incorporating non-carbon contaminants such as boron and nitrogen, the fabricated diamond can be rendered highly conductive [32,33] therefore attractive to be utilized for neural interfaces.

One drawback of using diamond for neural interfacing is that it typically exhibits very low electrochemical capacitance. Diamond has long been shown to exhibit a large water window but the small electrochemical capacitance of conventional diamond materials, and the corresponding low charge injection capacity results in a material that is generally not suitable for neural stimulation. Modified versions of diamond however have been found to be suitable for neural stimulation. For example, a device fabricated by The Bionic Vision Australia (BVA) consortium for restoring the sight of blind people utilizes nitrogen included ultrananocrystalline diamond (N-UNCD) as the conducting form of diamond for retinal stimulation, attached to the inner surface of the retina (epi-retinal) using a magnetic attachment method [34]. Previous results have reported the maximum charge injection capacity for the N-UNCD electrodes on the BVA device was 160 $\mu C/cm^2$ (after electrochemical activation [35]), a value that was later improved to 300 $\mu C/cm^2$ [36]. An *In vivo* study was subsequently conducted by Shivdasani et al. and they showed that a single 120 × 120 μm^2 square N-UNCD electrodes as part of an array, attached retinally, could elicit a response in the visual cortex of a cat with charge injections as low as 30 $\mu C/cm^2$ [37]. Some electrodes however required over 400 $\mu C/cm^2$ to elicit a response, higher than the safe charge injection capacity of the diamond (300 $\mu C/cm^2$). The term "charge injection capacity" is defined as the amount of charge that can be injected into the electrode before the voltage of the electrode exceeds a predetermined safe limit. Mathematically this is the equivalent of multiplying the electrochemical capacitance of the electrode by the maximum safe voltage. We have previously determined the safe voltage window for diamond as lying between −1.8 and 1.1 V [36] therefore the lower of these limits (1.1 V) is used to determine the charge injection capacity. Therefore, for diamond, charge injection capacity can be derived from capacitance by multiplying by 1.1 V.

In this paper, we report an increase in the electrochemical capacitance and therefore charge injection capacity of N-UNCD from 17 $\mu F/cm^2$ for the as-grown material, to more than 1000 $\mu F/cm^2$ after 3 h of treatment with low energy (50 W, 25% O_2 in argon) oxygen plasma, resulting in a charge injection capacity of more than 1 mC/cm^2. The origin for this increase, and the role of hybrid sp^2/sp^3 carbon in N-UNCD is one foci of this paper. We hypothesize that the increase in capacitance is due to the incorporation of oxygen functionalities followed by etching of the electrochemically active graphitic grain boundaries in the nanocrystalline diamond film. The *in vitro* biocompatibility of activated diamond was then assessed using primary rat cortical neurons and the surface morphology was found to be critical for neuron attachment and neurite outgrowth. The study not only provides a simple and efficient method for improving both the electrochemical and biological properties of N-UNCD films, it might also shed light on improving other forms of carbon materials for neural interface applications. Significantly the results provide a method of producing a diamond electrode that is optimized for both high charge injection capacity and biocompatibility.

2. Materials and methods

2.1. Diamond preparation

Synthesis of N-UNCD films: N-UNCD films were deposited onto 10 × 10 mm n-type Si (100) substrates (MMRC Pty Ltd) using an Iplas microwave plasma-assisted chemical vapor deposition system, as described previously [35]. Briefly, silicon substrates were seeded before deposition with nanodiamond (NanoArmor) by ultrasound in ~5 nm nanodiamond/methanol solution. A gas mixture of 79% argon, 20% nitrogen and 1% methane (All gases, BOC Australia, purity 99.999%) was used. During the growth, the microwave power was maintained at 1000 W, gas pressure at 90 Torr, and stage temperature at 900 °C. All the N-UNCD films were grown for 15 h, resulting in a film thickness of 6–8 μm and a conductivity (two-point measurement) of 46 S/cm.

Unless specifically mentioned, the experiments were conducted using the grown surfaces of the N-UNCD films without removing the silicon substrates. Some N-UNCD surfaces with low roughness were obtained by dissolving away the silicon substrates with an etchant solution (HF: HNO_3: CH_3COOH = 10:10:1) revealing the 'seeding' side of the diamond films which in general is smoother than the growth side.

After the N-UNCD synthesis, samples were placed in a Diener Femto plasma cleaner using a 3:1 argon: oxygen plasma at 45 sccm

with a power of 50 W for varying amounts of time from 0.5 min up to 7 h. Hydrogen plasma treatment was performed in an Iplas microwave plasma-assisted CVD system using a plasma power of 2000 W, a flow rate of 1000 sccm and a chamber pressure of 80 Torr for 1 min.

2.2. Electrochemical characterization

Electrochemical experiments were conducted on an EDAQ EA163 potentiostat using a purpose-built Teflon electrochemical chamber as previously described [35]. The N-UNCD electrodes were secured to the bottom of the chamber with a small area exposed to the electrolyte solution. The exposed area was approximately 0.196 cm^2 defined by an O-ring. The electrical contact to the N-UNCD electrodes was made using a copper wire glued to the surface with silver epoxy outside the area defined by the O-ring. A platinum wire counter electrode and an Ag/AgCl (1 M KCL) reference electrode was introduced through the chamber lid.

For measuring the electrochemical capacitance, cyclic voltammetry (CV) was conducted in pH 7.4 50 mM phosphate buffered saline (PBS, 0.13 M NaCl) at room temperature at scan rates from 10 to 50 mV/s over a voltage range from −100 mV to 100 mV *vs* Ag/AgCl. The capacitance was calculated, as previously described [35], according to the relationship $I = C\left(\frac{dV}{dt}\right)$, where I is the current (A), C is the specific capacitance (F), and dV/dt is the scan rate (V/s). The slope from the current magnitude of a series of cyclic voltammograms at a given potential (0 V in this instance) versus the scan rate therefore yields capacitance.

CV was also conducted for determining the water window in PBS at room temperature at scan rate of 100 mV/s over a voltage range from −2 V to 2 V vs Ag/AgCl. The maximum safely achievable charge injection capacity was calculated by multiplying the maximum voltage associated with the water window with the measured capacitance.

Electrochemical activation of the N-UNCD film was conducted by cyclic voltammetry in PBS from 0 to 2.5 V at a scan rate of 100 mV/s for various numbers of cycles. Deionized water was used for all experimental solutions.

2.3. Surface chemistry characterization

X-Ray Photoelectron Spectroscopy (XPS) data were collected in a Thermo-Fisher K-Alpha apparatus (10^{-9} mbar) using an Mg Kα radiation source at a power of 300 W using a 400 μm spot size and survey spectra measured at a 200 eV pass energy. Synchrotron NEXAFS experiments were conducted at the soft X-ray beamline at the Australian Synchrotron at a base pressure of 10^{-10} mbar and the total energy resolution better than 0.1 eV.

Near Edge X-ray Adsorption Fine Structure (NEXAFS) spectra were obtained in the partial electron yield (PEY) mode. The photon flux was monitored using the drain current from a half transparent gold mesh, allowing intensity and energy normalization across different scans.

2.4. Surface morphology characterization

Scanning Electron Microscopy (SEM) micrographs was obtained using an xT Nova Nanolab 200FIB/SEM apparatus operating under accelerating voltage of 5 kV, current of 98 pA, and working distance of approximately 5 mm.

Atomic Force Microscopy (AFM) was performed using an AFM CYPHER system under tapping mode. Surface roughness was assessed in a scanning area of 20 × 20 μm^2. Each sample was scanned in 3 different areas. Data was analyzed using Igro Pro software.

2.5. Biocompatibility assessment

Cultures of cortical neurons were obtained by isolating the cerebral cortices from one-day-old rats, as previously described [38]. Briefly, the heads were removed and placed in Hank's balanced salt solution (HBSS; Gibco). Then the skin and top of the skull were removed and a small area of cortex was pinched off with fine forceps. Meninges were removed and the tissue was chopped with a scalpel blade. The tissue was dissociated by protease digestion for 20 min at 37 °C using 10 μg/mL DNAse 1 (Sigma) and 250 μg/mL trypsin (Sigma) in HEPES buffered Eagles Medium. Trypsinisation was terminated by using Soybean Trypsin Inhibitor (Sigma) containing 10 μg/mL DNAse 1 and cells were pelleted by centrifuging and then triturated using a P1000 pipette. Finally, cells were diluted in culture medium (Neurobasal A with 2% B27 supplement, 2 mM Glutamax, 100 μg/mL penicillin and 100 μg/mL streptomycin; Gibco) and seeded onto diamond samples. The cell cultures were then incubated at 37 °C in 5% CO_2 for the required length of time.

After incubation for 24 h or 48 h, the cells were washed with PBS once and fixed in 4% paraformaldehyde in PBS for 10 min at room temperature, followed by cold (−20 °C) methanol for another 10 min. Then the cells were washed with PBS three times. After 30min in a blocking solution (2% fetal calf serum and 2% normal goat serum in PBS), the samples were incubated for 20min with primary antibody (mouse anti-beta-III tubulin; Promega) at room temperature. Samples were then washed with PBS and incubated with secondary antibody (Cy3-conjugated goat anti-mouse immunoglobulin; Jackson Immunolabs) and the nuclear stain DAPI for another 20 min. They were finally washed in triplicate with PBS and mounted for imaging. Images of neurons were acquired using a fluorescence microscope (Olympus BX60FS microscope with Olympus UplanFL 10x/0.3, 20x/0.5 and 40x/0.75 lenses and a digital camera (HRc and Axioviosion 4 software (Zeiss)).

Neuron density, neurite number per cell and neurite length was counted or measured for at least 5 randomly chosen areas per condition, per experiment, in at least three experiments. The cell number was counted automatically using software ImageJ and neurite lengths were measured by tracing individual neurites using the tool NeuronJ in ImageJ software. The results are expressed as average neuron density, average neurites per neuron and average longest neurite length. Statistical significance of the difference was determined using one-way ANOVA and a Bonferroni post hoc *t*-test.

3. Results and discussion

3.1. Electrochemical characterization

3.1.1. Electrochemical capacitance enhancement

Fig. 1a and b shows a series of cyclic voltammograms recorded using an N-UNCD electrode before and after a 3 h oxygen plasma treatment. To calculate the specific capacitance, the current magnitudes of these cyclic voltammograms at 0 V vs Ag/AgCl were plotted versus their respective scan rates (shown in Fig. 1c). The specific electrochemical capacitance was calculated by dividing the slopes by the exposed electrode area. The greater slope of the 3-h oxygen plasma treated sample in Fig. 1c indicates a larger electrochemical capacitance.

Cyclic voltammograms recorded in PBS over the potential range −2 to 2 V are shown in Fig. 1d, and are consistent in shape with CVs recorded previously on N-UNCD [35]. The onset of water oxidation for both types of diamond films occurs at $E \approx 1.3\ V$. The reduction of water occurs at potential more negative than $-1.8\ V$. The oxygen plasma treatment, up to 3 h, did not narrow the water window for N-UNCD. The apparently larger enclosed area in cyclic voltammogram for N-UNCD after 3-h oxygen plasma also indicates

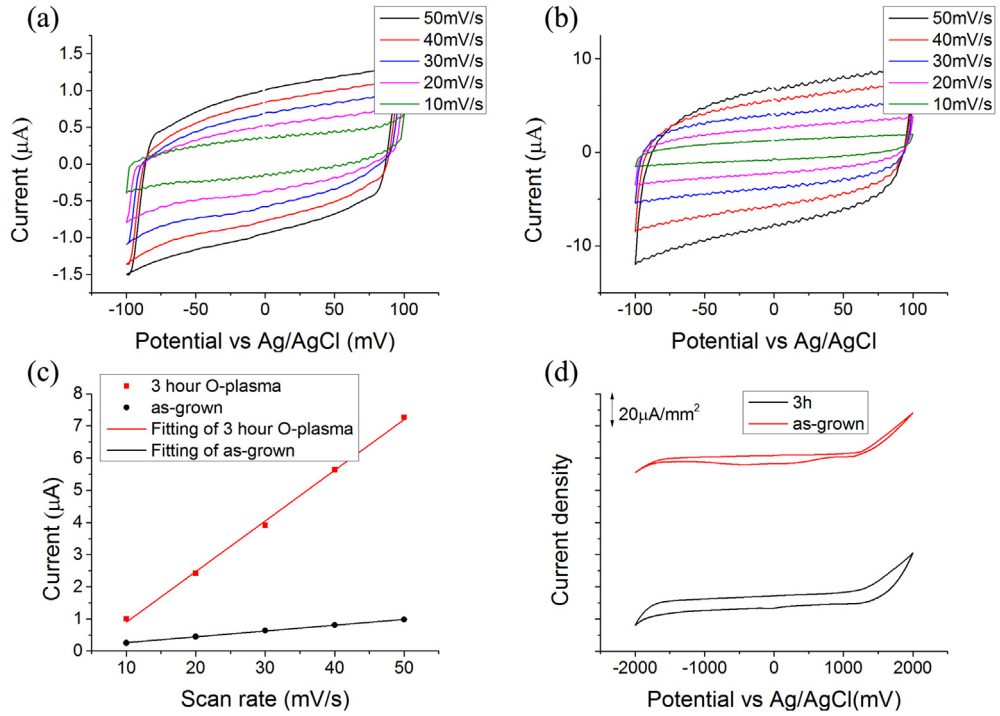

Fig. 1. Cyclic voltammograms recorded using the growth sides of N-UNCD electrodes before (a) and after 3-h oxygen plasma treatment (b) in PBS(c) The current width at 0 V for CVs shown in (a) and (b) plotted versus their respective scan rates. Note the different vertical scales in (a) and (b) The specific electrochemical capacitance was then calculated according to the slopes of linear fitting in (c) divided by the electrode area exposed to the PBS (0.196 cm^2). The oxygen plasma treatment didn't narrow the electrochemical water window as shown in (d) that both types of N-UNCD exhibit electrochemical water window from −1.8 V to 1.3 V. A larger enclosed area for N-UNCD after 3-h oxygen plasma indicates its larger electrochemical capacitance.

an increase in electrochemical capacitance in comparison with as-grown diamond films.

Fig. 2 shows the electrochemical capacitance of the growth sides of N-UNCD after different oxygen plasma treatment times (Red) and the electrochemical capacitance of the smooth (seeded) side of the diamond as produced (0 min) and after 180 min of oxygen plasma treatment (green). Also indicated (purple dashed lines) are a 180 min oxygen plasma treated sample after a 1 min hydrogen plasma treatment and an electrochemically activated sample. The measured capacitance of the as-grown N-UNCD films was 17 μF/cm^2. After 30 s of oxygen plasma treatment the electrochemical capacitance increased to 40 μF/cm^2. We have previously demonstrated that electrochemical activation enhances the measured capacitance of N-UNCD [35]. The term electrochemical activation of the N-UNCD film in this case refers to anodization of the film by cyclic voltammetry in PBS from 0 to 2.5 V at a scan rate of 100 mV/s repeatedly. The previously measured capacitance on electrochemically activated N-UNCD increased to 163 μF/cm^2 (as shown in Fig. 1, purple dashed line) [35], which is similar to the capacitance measured in these experiments on N-UNCD after 10 min oxygen plasma treatment. Samples exposed to the oxygen plasma for 3 h exhibited a capacitance of 1070 μF/cm^2, the highest capacitance values measured. This is an extraordinarily high value for diamond and is superior to some of the best performing high charge electrode materials, e.g. titanium nitride [39]. The enhancement of electrochemical capacitance was also confirmed using electrochemical impedance spectroscopy, as shown in the Supplementary Fig. S1. Further oxygen plasma treatment after 3 h appeared to slightly decrease the electrochemical capacitance.

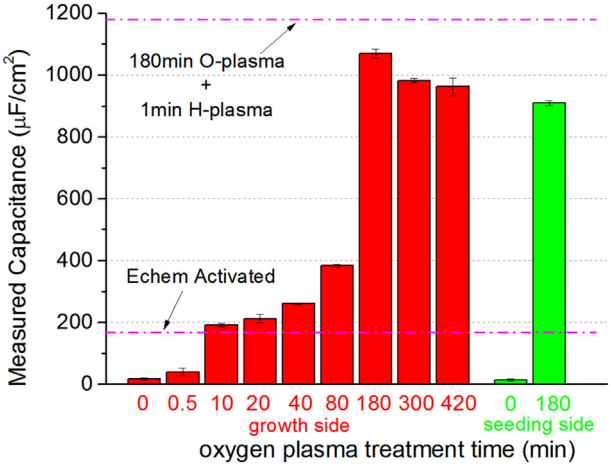

Fig. 2. Capacitance values for the growth sides of N-UNCD after oxygen plasma treatment for various lengths of time (red bars). Capacitance of the smooth, seeded side of the N-UNCD after 0 and 180 min of oxygen plasma (green bars). Also indicated are the capacitance of a 180 min oxygen plasma treated sample following a further 1 min in hydrogen plasma (purple dashed line) and the previously reported capacitance of electrochemical activated N-UNCD [35] (purple dashed line). Error bars are the standard deviation calculated from at least five measurements each from two sample electrodes. (For interpretation of the references to colour in this figure legend, the reader is referred to the web version of this article.)

The charge injection capacity of N-UNCD was calculated by multiplying the electrochemical capacitance with the water window. The safe water window is defined as voltages between −1.1 V and 1.1 V (well within the water electrolysis limits, −1.8–1.3 V) for N-UNCD with or without oxygen plasma activation. Therefore, the charge injection capacity of N-UNCD increased from approximately 20 μC/cm^2 for the as grown material to 1.18 mC/cm^2 as a result of the exposure to the oxygen plasma. The enhanced charge injection

capacity is more than 7 times that of the electrochemically activated N-UNCD (163 μC/cm^2) [35], and is larger than most neural stimulation materials [40].

3.1.2. Surface characterization

To investigate the possibility that changes in surface termination chemistry were responsible for the observed changes in capacitance, XPS was conducted on various N-UNCD samples using their grown surfaces. Survey spectra (Fig. 3a) taken before exposure to the oxygen plasma revealed a small amount of oxygen (~1–2%) on the surface. This oxygen most likely arises from exposure to air after removal from the growth chamber. The relative oxygen content increases to 12–13% after 5 min of plasma treatment (Fig. 3a), a figure which we have found to be consistent with a saturated level of oxygen on single-crystal diamond surfaces. Higher-resolution carbon-1s spectra (Fig. 3b) confirm that some of this oxygen was chemically bonded to the carbon, as seen by a chemically shifted peak due to C–O or O–C–O bonds at 286.5 eV [35,41]. The oxygen content then remains relatively constant after further oxidation, reaching a maximum of 14–15% for N-UNCD exposed to oxygen plasma for 3 h and longer. The C1s spectra on all samples did not change significantly after the first 5 min of oxygen plasma exposure. This strongly suggests that the N-UNCD surface is almost fully saturated with oxygen functionalities after 5 min of treatment.

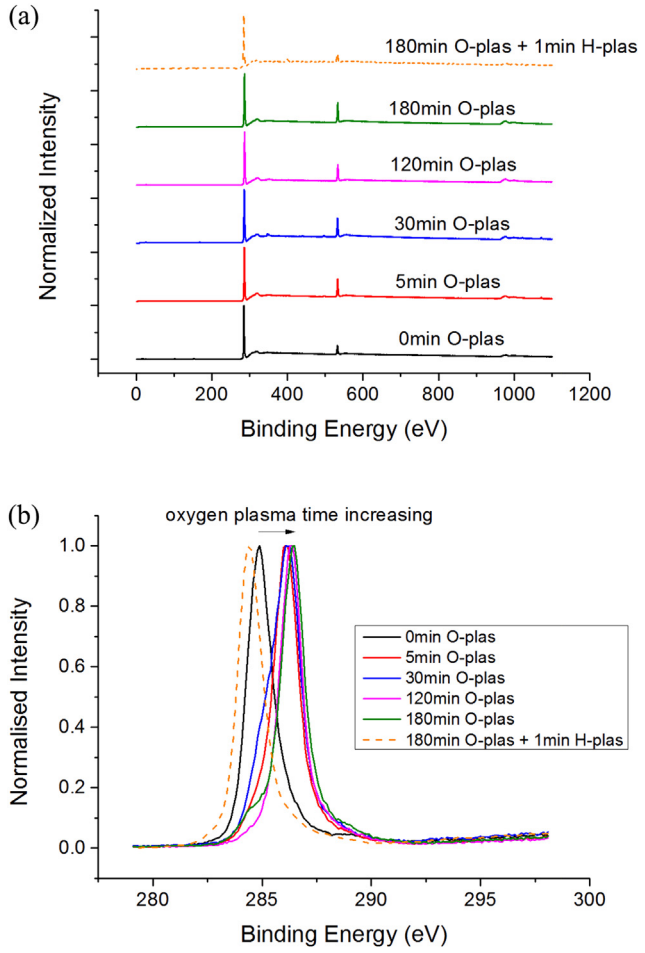

Fig. 3. XPS survey scans (a) and high resolution carbon 1s spectra (b) of the growth sides of N-UNCD films exposed to oxygen plasma and hydrogen plasma for different times, showing the incorporation of oxygen saturates within first 5 min and the removal of oxygen functional groups by hydrogen plasma.

The presence of oxygen functional groups has been reported to increase electrochemical capacitance of different materials [42–44]. It has been suggested that this may be due to increased hydrophilicity and in some cases, can also give rise to pseudocapacitance associated with reversible faradaic reactions, thus increasing the total capacitance at the electrode/electrolyte interface [45]. The oxidation of the film surface removes hydrogen and forms oxygen incorporated functional groups. The polar bonds such as C–O, O–C–OH and C–OH serve as adsorption sites for water [46] due to strong dipole-dipole interaction between polar molecules and the N-UNCD surface, potentially decreasing the thickness of the double layer at the interface. Therefore it is expected, due to this increased hydrophilicity, that the double layer capacitance will increase after oxygen plasma treatment [46]. These XPS results indicate that oxygen functionalization is saturated within 5 min of oxygen plasma treatment, and may account for some of the capacitance change during this time period. However the capacitance measurements continue to increase beyond 5 min of oxygen plasma, suggesting that the surface chemistry is not a sole factor in the overall increase in capacitance. This was confirmed by re-hydrogenation of a 3-h oxygen-plasma treated sample, using 1 min of hydrogen plasma. This process is known to remove oxygen functional groups and alter the surface back to hydrogen termination [47]. The removal of oxygen functional groups is also indicated from XPS in Fig. 3 that the oxygen content dropped after the additional hydrogen plasma and peak for the C1s spectrum shifted back to lower binding energy. Following hydrogen plasma treatment the electrochemical capacitance of the film remained high and in fact increased (as shown in Fig. 1, purple dashed line). We currently do not understand the increase in capacitance following hydrogen plasma however the result strongly suggests that oxygen functionalization is not the primary contributor to the enhancement of the capacitance on N-UNCD.

As an alternative to explain the large increase in surface capacitance for long term exposure to the O plasma, we considered the possibility that preferential etching of sp^2 bonded material in grain boundaries, known to occur in oxygen plasmas, might be responsible. The carbon bonding configuration at the sample surface was studied using surface-sensitive NEXAFS in PEY mode on the growth sides of N-UNCD films before and after oxygen plasma treatment. We have previously demonstrated that electrochemical activation enhances the capacitance of N-UNCD by introducing functional groups onto the surface [35] and hence include similar treated samples in this investigation for comparison. Spectra obtained from as-grown and electrochemically activated N-UNCD before oxygen plasma treatment indicate similar electronic structures (Fig. 4a). Both spectra show the expected features of diamond: a C 1s absorption edge slightly above 289 eV, a sharp core exciton peak at the onset of the absorption edge, and a distinct second band gap dip at 302.4 eV [47,48]. They also show prominent features associated with sp^2 bonding, which are at 285 eV corresponding to the π* antibonding state and σ* character with the peak onset at 291 eV [48]. The spectra for N-UNCD after exposure to oxygen plasma for 90 min (Fig. 4b) on the other hand exhibits a significantly less intense sp^2 bonded carbon π* and σ* resonance peak, compared to the as-grown N-UNCD film, but similar diamond exciton features. This suggests preferential etching of the sp^2 rich grain boundaries. Combining these studies, the increase of measured capacitance on N-UNCD after electrochemical activation appears to be mostly correlated to oxygen functionalization of carbon species while no significant loss in sp^2 bonded carbon is observed. The different spectra between electrochemical activated N-UNCD and the oxygen plasma treated N-UNCD however indicate they are quite different in their sp^2/sp^3 content, at the surface of the material.

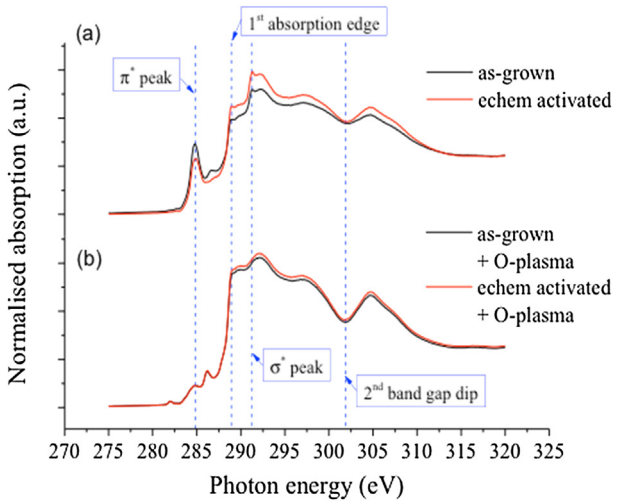

Fig. 4. NEXAFS spectra for growth sides of N-UNCD films. (a) shows NEXAFS scans for as-grown N-UNCD (black) and electrochemically activated N-UNCD (red). The diamond exciton and second band gap feature at 289.5 eV and 302.5 eV [47] remain similar after 90 min oxygen plasma on either as-grown (black) or electrochemically activated (red) N-UNCD (b) while the intensities of graphitic π^* and σ^* peaks decrease dramatically, indicating the selective etching of non-diamond in the grain boundaries. (For interpretation of the references to colour in this figure legend, the reader is referred to the web version of this article.)

Due to the etching of grain boundaries, the oxygen plasma might also roughen the film surface and create a more porous structure, thus increasing the effective surface area. Such enhancement due to increased effective surface area has been previously reported by several groups using different techniques. For example, Honda et al. reported giant capacitance of 1970 μF/cm^2 (geometric area) on boron-doped diamond by using porous alumina as mask for reactive ion etching to form a honeycomb structures [49]. When depositing boron-doped diamond on carbon cloth [50] or a carbon nanotube template [51] the capacitance could be increased 180 times or 450 times higher than that of diamond films on flat silicon substrates. All these increases were due to a large increase in the electrochemical surface area. Furthermore, oxygen plasma has previously shown potential for increasing the electrochemical surface area of diamond. Yang et al. fabricated diamond nanowires by using nanodiamond particles as a hard mask and using reactive ion etching in an O_2/CF_4 gas mixture [52]. By doing so, the surface area was increased to a maximum of 2.1 times the original area.

To assess the impact of oxygen plasma on surface morphology of the diamond high resolution SEM was utilized. Fig. 5 shows the growth sides of N-UNCD surface before and after 3 h of oxygen plasma treatment. When observing the surfaces using normal incidence, there is little observable difference between the samples before and after treatment. Both of the surfaces have fin-structured grains with length of about 100 nm and width of 5 nm. However, using a glancing angle of 52°, reveals a dramatic difference in the nanostructures of the N-UNCD surfaces before and after long oxygen plasma treatment. Nano cone structures can be observed clearly on the surfaces after 3 h of oxygen plasma exposure, but not before plasma etching. The cones have various heights, ranging from several nm up to about 100 nm. A real surface area enhancement is therefore apparent, which can change the electrochemical behaviors accordingly.

The increase of surface area was also indicated from the change of surface roughness measured on N-UNCD before and after oxygen plasma exposure. A set of rough (growth) and smooth (seeded) diamond surfaces were oxidized for 5 min and 3 h and the average surface roughness for each surface was characterized using AFM, as shown in Fig. 6. The surface roughness increased on both types of N-UNCD films after oxidation. The average roughness of rough diamond increased from 75.8 nm to 84.4 nm after 5 min oxidation, and reached 117.4 nm with 3 h plasma exposure. The average roughness of smooth diamond was 3.2 nm, 7.5 nm and 21.7 nm for the untreated, 5 min and 3 h plasma treated surfaces, respectively. The increase of surface roughness therefore indicated that the effect of surface area increase by extended oxygen plasma is similar for both types of diamond surfaces. The increases in surface roughness are insufficient however to account for the very large increase in capacitance therefore we speculate that there is significance nano roughness below the measurement capabilities of AFM.

3.1.3. Possible mechanism

Combining the surface chemistry and surface morphology characterization of the oxidized N-UNCD, a mechanism for the capacitance enhancement can be proposed based on changes to the hybrid sp^2/sp^3 carbon structure, as shown in Fig. 7. There are two steps for the increase of the measured electrochemical capacitance.

Within the first 5 min oxygen plasma exposure, the predominantly hydrogen terminated N-UNCD surfaces are transformed into oxygen terminated surfaces due to the incorporation of oxygen functional groups onto the N-UNCD surfaces (Fig. 7a,b). XPS indicates that the percentage of oxygen in the survey spectra increases dramatically on the 5 min oxygen plasma treated samples. We have previously shown that the water contact angle of 5 min oxygen plasma treated samples dropped from 104° for as grown to 27° after 5 min of exposure to the plasma [28], indicating an increase in hydrophilicity and likely decrease of double layer thickness at the diamond-solution interface. Consequently, the electrochemical capacitance increases from 20 μF/cm^2 to over 100 μF/cm^2 after 10 min oxygen plasma treated samples.

After 5 min of oxygen plasma treatment the oxygen termination is saturated and the major effect of further plasma treatment is the etching of N-UNCD surfaces (Fig. 7c). According to the SEM images, there are cone structures formed on the N-UNCD surfaces, indicating a surface area enlargement. The huge surface area increase is associated with the sp^2/sp^3 hybridization of N-UNCD in that sp^2-bonded grain boundaries is preferentially etched by oxygen plasma, as indicated by NEXAFS. This increase is thus unlikely to happen on surfaces composed with mono-chemical structures such as pure sp^3 or sp^2 bonded carbon, on which the plasma etching effect is uniform across the entire surface. As a result, the ratio between the effective and geometric surface area increases significantly on N-UNCD after extended oxidation, leading to the increase of measured electrochemical capacitance.

Although the mechanism presented above about the surface area enlargement with extended oxygen plasma is sufficient for explaining the capacitance or charge injection capacity enhancement for N-UNCD electrodes, the special sp^2/sp^3 hybrid structures formed after 3 h oxygen plasma exposure may also play an important role, according to the AFM roughness measurements. This is due to the similar electrochemical properties, but significantly different surface roughness observed on both smooth and rough samples oxidized for 3 h. Assuming that surface roughness and real surface area is positively correlated, the oxidized smooth N-UNCD (RMS: 21.7 nm) should have real surface area much smaller than oxidized rough surfaces (RMS: 117.4 nm), which is however inconsistent with their observed capacitance relationship. On the contrary, their surface sp^2/sp^3 hybridization is identical, thus may be a contributor to the observed huge capacitance. Nevertheless, no matter the relative importance of the surface area enhancement or the final sp^2/sp^3 hybridization in

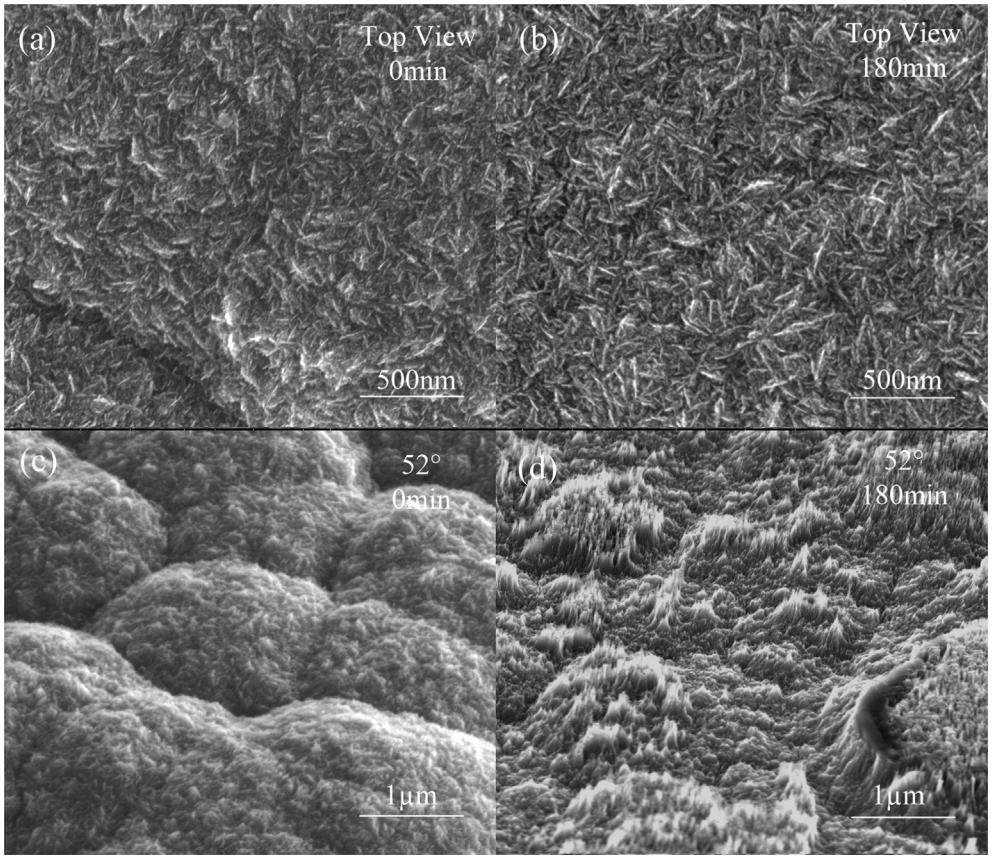

Fig. 5. High resolution SEM images of the growth sides of N-UNCD before (a,c) and after 3 h oxygen plasma treatment (b,d), observed from top view (a,b) and from an angle of 52° (c,d).

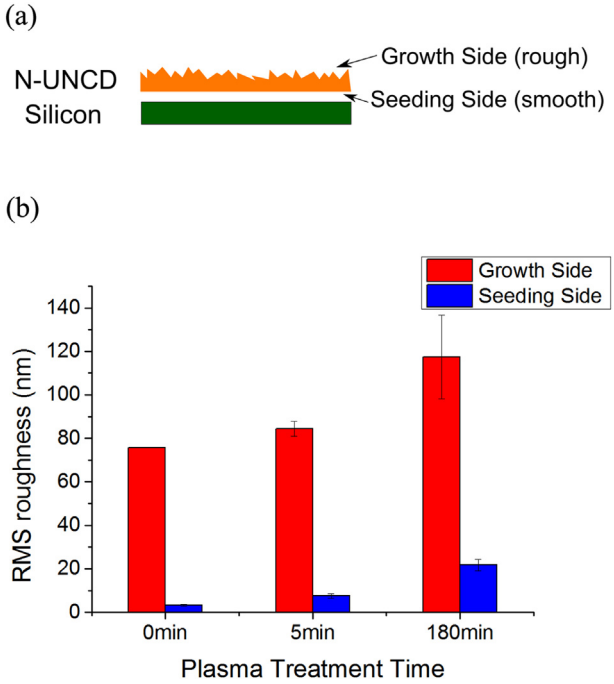

Fig. 6. Schematic illustration of the fabrication of rough and smooth N-UNCD diamond surfaces (a). AFM shows that the RMS roughness for both rough and smooth N-UNCD increased after oxygen plasma treatment (b). Values expressed are means (n = 3) ± standard deviation.

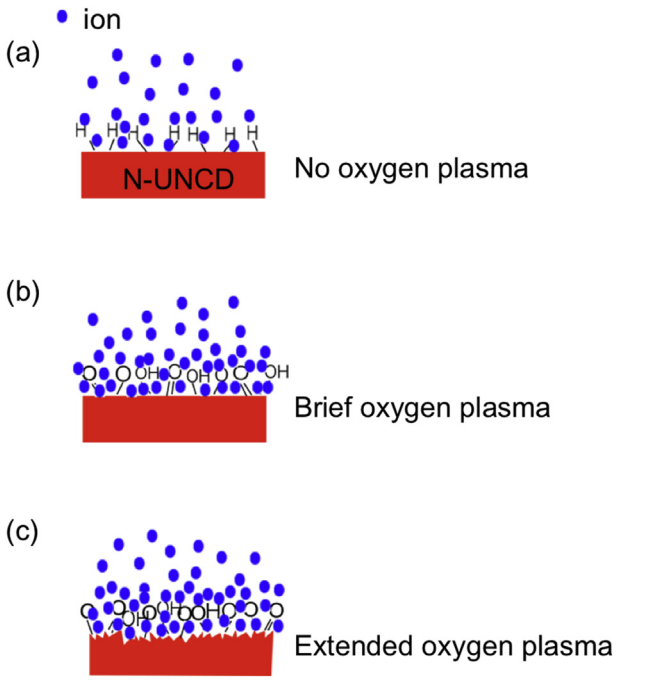

Fig. 7. Schematic of N-UNCD surface change induced by oxygen plasma treatment. The N-UNCD is composed of diamond grains and non-diamond grain boundaries. Double layer capacitors form at the electrode/electrolyte interface. After short oxygen plasma treatment, the surface of the as-grown N-UNCD (a) is changed from hydrogen termination to oxygen termination (b). Further oxygen plasma etches the non-diamond grain boundaries, thus dramatically increasing the effective surface area (c).

determining the extremely high capacitance, both of these factors are closely linked with the unique hybrid sp^2/sp^3 structure of the as-grown N-UNCD.

3.2. Biocompatibility assessment

3.2.1. In vitro neuron culture on oxidized growth side of diamond

The increase in charge injection capacity is a necessary but not by itself a sufficient condition for the use of N-UNCD as an electrode. It is also necessary to consider the biological interaction of neurons with these modified surfaces. Therefore the biocompatibility of the growth sides of N-UNCD films was assessed using primary rat cortical neurons without pre-coating the diamond surfaces with any additional chemicals. Fig. 8a–e shows typical fluorescence images of neurons on different diamond surfaces after 48 h of incubation. The images show that the neurons survived on the as-grown, 5 min and 30min oxygen plasma treated surfaces. Few neurons survived however on diamond surfaces that were exposed to oxygen plasma for more than 2 h.

Statistical analysis of the neuron density and neurite outgrowth on the as-grown and 5 min or 30min oxygen plasma treated surfaces are summarized in Fig. 8f–h. The cell density showed no significant difference. However, the surfaces exposed to 5 min oxygen plasma appeared to be a somewhat better substrate than the as-grown surfaces for the neurite outgrowth, which showed significantly more neurites per neuron in comparison with those on the as-grown samples. The results also suggested that both 5 min and 30min oxygen plasma treated samples produced extended neurites, significantly longer than those on the as-grown samples. The average length for the longest neurite per neuron was even longer for the 5 min oxygen plasma samples than that on the 30min oxygen plasma samples. Therefore, the surfaces that were exposed to 5 min oxygen plasma supported neuron growth the most.

3.2.2. The effect of surface roughness

The XPS results indicate that for the growth sides of N-UNCD increasing the oxygen plasma treatment after the initial 5 min does not induce significant difference in its surface chemistry. However, according to SEM and AFM characterization, the diamond surface was etched by extended oxygen plasma, changing its surface roughness.

In order to determine whether surface roughness is responsible for the differences in neuron growth on the brief and extended oxygen plasma treated samples, the biocompatibility assessment was repeated on the low surface roughness side of similar diamond films. Fig. 9a–f shows the neurons after 48-h incubation on the growth (rough) or seeded (smooth) side of diamond films before and after the same period of oxygen plasma exposure. Consistent with the results shown in section 3.2.1, there was no cell survival on the 3-h oxygen treated rough surfaces. In addition, the neurons on 5 min rough surfaces extended more branches and longer neurites compared with those on the as-grown rough surfaces.

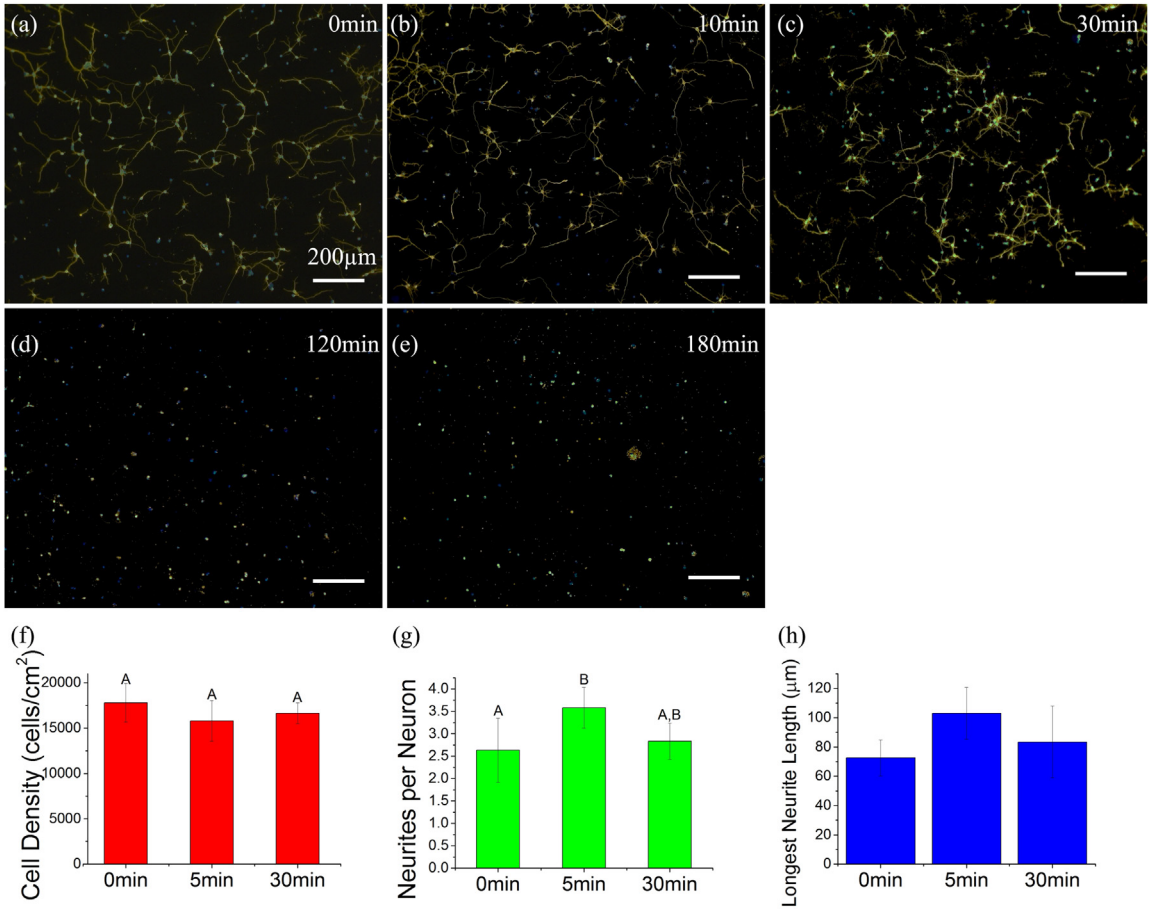

Fig. 8. Fluorescence images of primary rat cortical neuron adhesion and growth on the growth sides of N-UNCD before and after oxygen plasma treatment after 48-h incubation (a–e). Statistical results of cell density, number of neurites per neuron and longest neurite length on the as-grown diamond films, or diamond films after 5 min or 30min oxygen plasma treatment are summarized in (f–h). The bars show the mean value ± the standard deviation. Letters shared in common between or among the groups indicate no significant difference. $p < 0.05$.

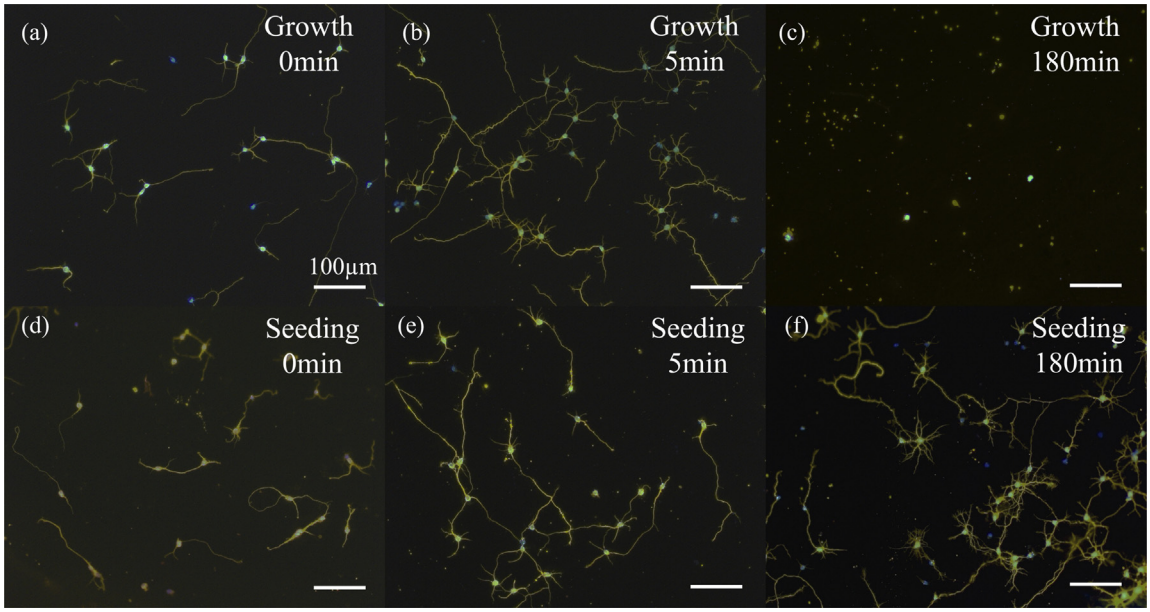

Fig. 9. Fluorescence images of primary rat cortical neuron adhesion and growth on either rough (growth) (a–c) or smooth (seeded) (d–f) N-UNCD before and after oxygen plasma treatment after 48-h incubation. Statistical results of cell density, number of neurites per neuron and longest neurite length are summarized in Fig. 10.

In contrast with the results on diamond with rough surfaces, the neurons survived after 48-h incubation on all smooth surfaces, even for those exposed to oxygen plasma for 3 h. The neurons on the oxidized smooth samples extended more branches and longer neurites in comparison with those on the untreated smooth surfaces.

Fig. 10 show the statistical results of neurons adhered onto both rough and smooth N-UNCD surfaces before and after oxygen plasma treatment, The cell densities on N-UNCD oxidized for 5 min showed no significant difference from those on N-UNCD without oxidation, regardless of their surface roughness. In comparison, the smooth surface after 3-h oxidation showed greater cell densities

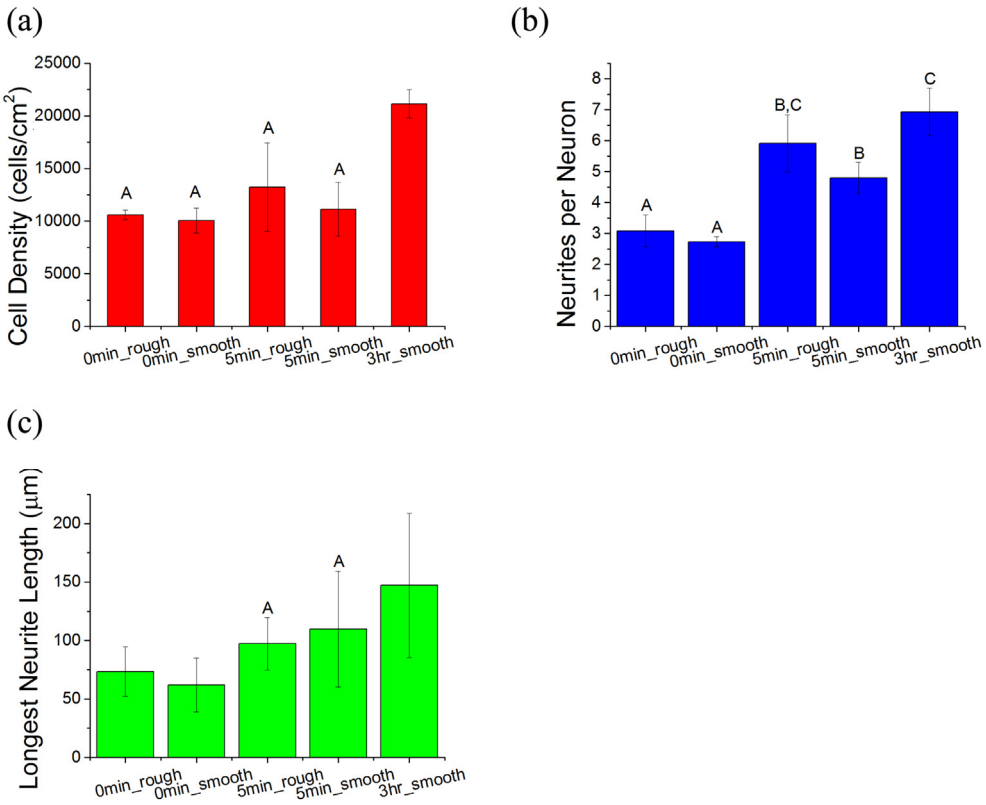

Fig. 10. Statistical results of cell density, number of neurites per neuron and longest neurite length on smooth and rough samples with or without oxygen plasma activation. The bars show the mean value ± the standard deviation. Letters shared in common between or among the groups indicate no significant difference. $p < 0.05$.

than all the other surfaces. Five minute oxygen plasma significantly increased the number of neurites per neuron on both smooth and rough surfaces. However, the average number of neurites per neuron was increased to even greater value on the 3-h oxidized smooth surfaces. Furthermore, the neurons on the 3-h smooth samples also extended neurites with longest average length.

Therefore, the death of neurons on the extended plasma treated rough surfaces was likely associated with the very high surface roughness and or specific morphology of those surfaces. These different results on the smooth and rough diamond surface indicate that the neurons can sense the nano-structure of the diamond surfaces and these differences in turn mediate the neuron growth and neurite outgrowth. Brief oxygen plasma resulted in the change of surface termination leading to increased hydrophilicity of N-UNCD surfaces, and lead to the increase of neurite branches as well as the length of the longest neurites. The N-UNCD before oxygen plasma has a surface roughness of 75.8 nm, and on this surface the neurons showed poor survival on the extended oxygen plasma treated surfaces, probably due to the great increase of surface roughness induced by long term plasma etching. However, if the N-UNCD without oxygen plasma was much smoother and shared a similar surface roughness with polished silicon (~3.2 nm), the neurons on these surfaces oxidized for 3 h extended even more branches and longer neurites in comparison to those on N-UNCD with short oxygen plasma exposure. Considering that high capacitance was also observed on smooth samples treated with oxygen plasma for 3 h, this is a significant result as it represents a material that is optimized for both charge injection capacity and biocompatibility.

Neurons have been shown to be able to sense the nano roughness of different materials [53,54]. For example, Brunetti et al. investigated the response of a human neuroblastoma cell line to gold surfaces with different levels of nanoroughness [53]. In the research, they demonstrated that neurons sensed and actively responded to the surface nanotopography, with a surprising sensitivity to variations of a few nanometers. They also suggested that the observed cell response could be explained by the properties of nanorough surfaces to influence the adsorption of cell adhesive serum proteins, such as fibronectin and laminin, in terms of composition and/or correct folding of the adsorbed protein layer. This class of proteins plays a critical role in neuron adhesion and growth. The hypothesis can be applied to the explanation of the results in our experiments that cells survived on smooth N-UNCD surfaces after long oxygen plasma treatment but died on rough surfaces with the same amount of oxygen plasma treatment. The surface nanostructure may be responsible for the different preference of neurons and such preference may actually be a consequence of different protein adsorption capacities of these surfaces. In another study, Fan et al. showed that neurons showed optimal growth on silicon surfaces with an average roughness ranging from 20 to 50 nm [54]. The cell adherence however was adversely affected on surfaces with average roughness less than 10 nm or above 70 nm in good agreement with our observations during the work discussed here. For N-UNCD after oxygen plasma exposure, their average roughness sequence is: 3-h rough (117.4 nm) > 5-min rough (84.4 nm) > 3-h smooth (21.7 nm) > 5-min smooth (7.5 nm). It is possible that the surface roughness of 3-h smooth samples was in the range of the optimal surface roughness for neuron growth on N-UNCD. At the same time, the roughness for 3-h rough samples may already fall into the region that neuron growth is adversely affected.

Combining the electrochemical and neuron growth results, both the charge injection capacity and biocompatibility of N-UNCD was enhanced greatly using smooth N-UNCD and extended oxygen plasma activation.

4. Conclusion

We have examined the impact of oxygen plasma treatment on the electrochemical properties and biocompatibility of N-UNCD films and discovered optimized conditions that produce a diamond electrode with high charge injection (>1 mC/cm^2) and a surface morphology that promotes healthy neuron growth (≈20 nm RMS roughness). The electrochemical capacitance and the charge injection capacity of N-UNCD films increased dramatically and reached a maximum after 3 h of low power oxygen plasma treatment. A model for the origin of increased electrochemical capacitance in oxidized N-UNCD films was proposed taking into account the effects of oxygen plasma on carbon materials and the special hybrid sp^2/sp^3 structure of N-UNCD films. We propose that the oxygen plasma increased the double layer capacitance between the electrode/electrolyte interfaces by initially oxygen functionalizing the N-UNCD films. After oxygen functionalization is saturated within the first 5 min, the electrochemical capacitance continued to increase due to removal of the graphite component in N-UNCD grain boundaries, resulting in an increased effective surface area. The biocompatibility of N-UNCD was then assessed using rat cortical neurons. Optimal neuron growth was found to be highly affected by the roughness of the diamond surfaces with best growth occurring on diamond with an RMS roughness of ≈20 nm. Therefore, by using N-UNCD with appropriate surface roughness and appropriate oxygen plasma activation, both its electrochemical properties and biocompatibility can be greatly improved. Both properties are highly beneficial for fabrication of diamond neural interfaces with the expected long-term stability of diamond whilst supporting a healthy neuron/electrode interface.

Acknowledgement

The authors wish to acknowledge the facilities and the scientific assistance of the Australian Microscopy & Microanalysis Research Facility at the RMIT Microscopy & Microanalysis Facility at RMIT University, and the Australian Synchrotron. A part of this research was undertaken on the Soft X-ray beamline at the Australian Synchrotron, Victoria, Australia. DJG is supported by an Australian Research Council (ARC) DECRA grant DE130100922. This research was supported by the ARC through its Special Research Initiative (SRI) in Bionic Vision Science and Technology grant to Bionic Vision Australia (BVA).

Appendix A. Supplementary data

Supplementary data related to this article can be found at http://dx.doi.org/10.1016/j.biomaterials.2016.07.006.

References

[1] B.S. Wilson, C.C. Finley, D.T. Lawson, R.D. Wolford, D.K. Eddington, W.M. Rabinowitz, Better speech recognition with cochlear implants, Nature 352 (1991) 236–238.
[2] A. Caspi, J.D. Dorn, K.H. McClure, M.S. Humayun, R.J. Greenberg, M.J. McMahon, Feasibility study of a retinal prosthesis: spatial vision with a 16-electrode implant, Archiv. Ophthalmol. 127 (2009) 398–401.
[3] E. Zrenner, Will retinal implants restore vision? Science 295 (2002) 1022–1025.
[4] T. Cameron, G.E. Loeb, R. Peck, J.H. Schulman, P. Strojnik, P.R. Troyk, Micromodular implants to provide electrical stimulation of paralyzed muscles and limbs, Biomed. Eng. IEEE Trans. 44 (1997) 781–790.
[5] R.E. Gross, A.M. Lozano, Advances in neurostimulation for movement disorders, Neurol. Res. 22 (2000) 247–258.
[6] W. Grill, Signal Considerations for Chronically Implanted Electrodes for Brain Interfacing, 2008.
[7] S.G. Mason, A. Bashashati, M. Fatourechi, K.F. Navarro, G.E. Birch, A comprehensive survey of brain interface technology designs, Ann. Biomed. Eng. 35 (2007) 137–169.

[8] W.F. Agnew, Effects of prolonged electrical stimulation of the central nervous system, Neural Prosthes. Fundam. Stud. (1990) 225–252.
[9] R. Biran, D.C. Martin, P.A. Tresco, Neuronal cell loss accompanies the brain tissue response to chronically implanted silicon microelectrode arrays, Exp. Neurol. 195 (2005) 115–126.
[10] S. Stoney, W. Thompson, H. Asanuma, Excitation of pyramidal tract cells by intracortical microstimulation: effective extent of stimulating current, J. Neurophysiol. 31 (1968) 659–669.
[11] S. Brummer, M. Turner, Electrochemical considerations for safe electrical stimulation of the nervous system with platinum electrodes, Biomed. Eng. IEEE Trans. (1977) 59–63.
[12] D.R. Merrill, M. Bikson, J.G. Jefferys, Electrical stimulation of excitable tissue: design of efficacious and safe protocols, J. Neurosci. Meth. 141 (2005) 171–198.
[13] S.F. Cogan, Neural stimulation and recording electrodes, Annu Rev. Biomed. Eng. 10 (2008) 275–309.
[14] X. Cui, V.A. Lee, Y. Raphael, J.A. Wiler, J.F. Hetke, D.J. Anderson, et al., Surface modification of neural recording electrodes with conducting polymer/biomolecule blends, J. Biomed. Mater Res. 56 (2001) 261–272.
[15] W. Agnew, T. Yuen, D. McCreery, L. Bullara, Histopathologic evaluation of prolonged intracortical electrical stimulation, Exp. Neurol. 92 (1986) 162–185.
[16] G.M. Clark, R.J. Hallworth, A multiple-electrode array for a cochlear implant, J. Laryngol. Otol. 90 (1976) 623–627.
[17] G.W. Gross, Simultaneous single unit recording in vitro with a photoetched laser deinsulated gold multimicroelectrode surface, Biomed. Eng. IEEE Trans. (1979) 273–279.
[18] S. Li, C.W. Macosko, H.S. White, Electrochemical Processing of Conducting Polymer Fibers, Science, (Washington, DC);(United States), 1993, p. 259.
[19] G. Shi, C. Li, Y. Liang, High-strength conducting polymers prepared by electrochemical polymerization in boron trifluoride diethyl etherate solution, Adv. Mater 11 (1999) 1145–1146.
[20] J. Reeder, M. Kaltenbrunner, T. Ware, D. Arreaga-Salas, A. Avendano-Bolivar, T. Yokota, et al., Mechanically adaptive organic transistors for implantable electronics, Adv. Mater 26 (2014) 4967–4973.
[21] D.P. Nair, N.B. Cramer, T.F. Scott, C.N. Bowman, R. Shandas, Photopolymerized thiol-ene systems as shape memory polymers, Polymer 51 (2010) 4383–4389.
[22] A. Pud, Stability and degradation of conducting polymers in electrochemical systems, Synth. Met. 66 (1994) 1–18.
[23] D.J. Garrett, W. Tong, D.A. Simpson, H. Meffin, Diamond for neural interfacing: a review, Carbon 102 (2016) 437–454.
[24] A. Ahnood, A.N. Simonov, J.S. Laird, M.I. Maturana, K. Ganesan, A. Stacey, et al., Transient photoresponse of nitrogen-doped ultrananocrystalline diamond electrodes in saline solution, Appl. Phys. Lett. 108 (2016) 104103.
[25] L. Tang, C. Tsai, W. Gerberich, L. Kruckeberg, D. Kania, Biocompatibility of chemical-vapour-deposited diamond, Biomaterials 16 (1995) 483–488.
[26] D.J. Garrett, A.L. Saunders, C. McGowan, J. Specks, K. Ganesan, H. Meffin, et al., In vivo biocompatibility of boron doped and nitrogen included conductive-diamond for use in medical implants, J. Biomed. Mater. Res. Part B Appl. Biomater. 104 (2016) 19–26.
[27] B. Shi, Q. Jin, L. Chen, A.S. Woods, A.J. Schultz, O. Auciello, Cell growth on different types of ultrananocrystalline diamond thin films, J. Funct. Biomater. 3 (2012) 588–600.
[28] W. Tong, P.A. Tran, A.M. Turnley, M. Aramesh, S. Prawer, M. Brandt, et al., The influence of sterilization on nitrogen-included ultrananocrystalline diamond for biomedical applications, Mater. Sci. Eng. C 61 (2016) 324–332.
[29] L. Yang, B.W. Sheldon, T.J. Webster, The impact of diamond nanocrystallinity on osteoblast functions, Biomaterials 30 (2009) 3458–3465.
[30] L. Marcon, A. Addad, Y. Coffinier, R. Boukherroub, Cell micropatterning on superhydrophobic diamond nanowires, Acta Biomater. 9 (2013) 4585–4591.
[31] S. Kelly, E.M. Regan, J.B. Uney, A.D. Dick, J.P. McGeehan, E.J. Mayer, et al., Patterned growth of neuronal cells on modified diamond-like carbon substrates, Biomaterials 29 (2008) 2573–2580.
[32] S. Bhattacharyya, O. Auciello, J. Birrell, J.A. Carlisle, L.A. Curtiss, A.N. Goyette, et al., Synthesis and characterization of highly-conducting nitrogen-doped ultrananocrystalline diamond films, Appl. Phys. Lett. 79 (2001) 1441–1443.
[33] J. Xu, M.C. Granger, Q. Chen, J.W. Strojek, T.E. Lister, G.M. Swain, Peer reviewed: boron-doped diamond thin-film electrodes, Anal. Chem. 69 (1997) 591A, 7A.
[34] K. Fox, H. Meffin, O. Burns, C.J. Abbott, P.J. Allen, N.L. Opie, et al., Development of a magnetic attachment method for bionic eye applications. Artif. Organs 40 (2015) E12–E24.
[35] D.J. Garrett, K. Ganesan, A. Stacey, K. Fox, H. Meffin, S. Prawer, Ultra-nanocrystalline diamond electrodes: optimization towards neural stimulation applications, J. Neural Eng. 9 (2012).
[36] A.E. Hadjinicolaou, R.T. Leung, D.J. Garrett, K. Ganesan, K. Fox, D.A.X. Nayagam, et al., Electrical stimulation of retinal ganglion cells with diamond and the development of an all diamond retinal prosthesis, Biomaterials 33 (2012) 5812–5820.
[37] M. Shivdasani, D. Garrett, D. Nayagam, J. Villalobos, P. Allen, A. Saunders, et al., In vivo electrical stimulation of a retinal prosthesis containing conductive diamond electrodes, Investig. Ophthalmol. Vis. Sci. 54 (2013) 1029.
[38] Y. Goldshmit, C.J. Greenhalgh, A.M. Turnley, Suppressor of cytokine signalling-2 and epidermal growth factor regulate neurite outgrowth of cortical neurons, Eur. J. Neurosci. 20 (2004) 2260–2266.
[39] J.D. Weiland, D.J. Anderson, M.S. Humayun, In vitro electrical properties for iridium oxide versus titanium nitride stimulating electrodes, IEEE T Bio-Med Eng. 49 (2002) 1574–1579.
[40] S.F. Cogan, Neural stimulation and recording electrodes, Annu Rev. Biomed. Eng. 10 (2008) 275–309.
[41] S. Al-Riyami, S. Ohmagari, T. Yoshitake, X-ray photoemission spectroscopy of nitrogen-doped UNCD/a-C: H films prepared by pulsed laser deposition, Diam. Relat. Mater 19 (2010) 510–513.
[42] K. Okajima, K. Ohta, M. Sudoh, Capacitance behavior of activated carbon fibers with oxygen-plasma treatment, Electrochim. Acta 50 (2005) 2227–2231.
[43] C.C. Lin, H.C. Huang, Radio frequency oxygen-plasma treatment of carbon nanotube electrodes for electrochemical capacitors, J. Power Sources 188 (2009) 332–337.
[44] C.C. Lin, C.C. Yen, RF oxygen plasma treatment of activated carbon electrodes for electrochemical capacitors, J. Appl. Electrochem 37 (2007) 813–817.
[45] M.J. Bleda-Martinez, J.A. Macia-Agullo, D. Lozano-Castello, E. Morallon, D. Cazorla-Amoros, A. Linares-Solano, Role of surface chemistry on electric double layer capacitance of carbon materials, Carbon 43 (2005) 2677–2684.
[46] Y.T. Kim, Y. Ito, K. Tadai, T. Mitani, U.S. Kim, H.S. Kim, et al., Drastic change of electric double layer capacitance by surface functionalization of carbon nanotubes, Appl. Phys. Lett. 87 (2005).
[47] A.V. Sumant, D.S. Grierson, J.E. Gerbi, J. Birrell, U.D. Lanke, O. Auciello, et al., Toward the ultimate tribological interface: surface chemistry and nanotribology of ultrananocrystalline diamond, Adv. Mater 17 (2005) 1039.
[48] J. Birrell, J.E. Gerbi, O. Auciello, J.M. Gibson, D.M. Gruen, J.A. Carlisle, Bonding structure in nitrogen doped ultrananocrystalline diamond, J. Appl. Phys. 93 (2003) 5606–5612.
[49] K. Honda, T.N. Rao, D.A. Tryk, A. Fujishima, M. Watanabe, K. Yasui, et al., Electrochemical characterization of the nanoporous honeycomb diamond electrode as an electrical double-layer capacitor, J. Electrochem Soc. 147 (2000) 659–664.
[50] L.L.G. Silva, N.G. Ferreira, E.J. Corat, Morphological and electrochemical properties of boron-doped diamond films on carbon cloths with enhanced surface area, Thin Solid Films 516 (2008) 4934–4939.
[51] H. Zanin, P.W. May, D.J. Fermin, D. Plana, S.M.C. Vieira, W.I. Milne, et al., Porous boron-doped diamond/carbon nanotube electrodes, ACS Appl. Mater. Interfaces 6 (2013) 990–995.
[52] N.J. Yang, H.S. Uetsuka, E. Sawa, C.E. Nebel, Vertically aligned nanowires from boron-doped diamond, Nano Lett. 8 (2008) 3572–3576.
[53] V. Brunetti, G. Maiorano, L. Rizzello, B. Sorce, S. Sabella, R. Cingolani, et al., Neurons sense nanoscale roughness with nanometer sensitivity, P Natl. Acad. Sci. U. S. A. 107 (2010) 6264–6269.
[54] Y.W. Fan, F.Z. Cui, S.P. Hou, Q.Y. Xu, L.N. Chen, I.S. Lee, Culture of neural cells on silicon wafers with nano-scale surface topograph, J. Neurosci. Meth. 120 (2002) 17–23.